Velocity-jump models with crowding effects

Katrina K. Treloar,[1,2] Matthew J. Simpson,[1,2] and Scott W. McCue[1]

[1]*School of Mathematical Sciences, Queensland University of Technology, Brisbane, Queensland 4001, Australia*

[2]*Tissue Repair and Regeneration Program, Institute of Health and Biomedical Innovation, Queensland University of Technology, Brisbane, Queensland 4001, Australia*

(Received 13 October 2011; published 28 December 2011)

Velocity-jump processes are discrete random-walk models that have many applications including the study of biological and ecological collective motion. In particular, velocity-jump models are often used to represent a type of persistent motion, known as a run and tumble, that is exhibited by some isolated bacteria cells. All previous velocity-jump processes are noninteracting, which means that crowding effects and agent-to-agent interactions are neglected. By neglecting these agent-to-agent interactions, traditional velocity-jump models are only applicable to very dilute systems. Our work is motivated by the fact that many applications in cell biology, such as wound healing, cancer invasion, and development, often involve tissues that are densely packed with cells where cell-to-cell contact and crowding effects can be important. To describe these kinds of high-cell-density problems using a velocity-jump process we introduce three different classes of crowding interactions into a one-dimensional model. Simulation data and averaging arguments lead to a suite of continuum descriptions of the interacting velocity-jump processes. We show that the resulting systems of hyperbolic partial differential equations predict the mean behavior of the stochastic simulations very well.

DOI: 10.1103/PhysRevE.84.061920 PACS number(s): 87.10.Rt, 87.17.Aa, 87.17.Jj, 87.17.Rt

I. INTRODUCTION

Discrete random-walk models are well suited to studying collective cell migration [1–3]. These models provide us with detailed spatiotemporal snapshots and sequences of images that are easy to compare with experimental time-lapse data [4]. There are two key classes of lattice-based random-walk models that have been used to represent collective cell migration.

Position-jump processes are a class of random-walk model in which the location of each agent undergoes a series of discrete jumps [1,2,4,5]. Typically, a position-jump model involves simulating a population of agents on a regular lattice, with lattice spacing Δ. During each discrete time interval of duration τ, all agents are given the opportunity to change position with probability $P \in [0,1]$. Changes in position are usually represented by nearest-neighbor transitions and the choice of target site can be unbiased (undirected) or biased (directed). Traditional position-jump models are *noninteracting* [2,6], which means that each motility event is independent of the state of the system. For example, an agent could step to a target site that is already occupied so that multiple agents reside at the same location. A population-level description of a noninteracting position-jump model can be derived by constructing a discrete conservation statement and then considering the limit in which $\Delta \to 0$ and $\tau \to 0$ simultaneously [1]. For a noninteracting unbiased position-jump processes, this leads to the linear diffusion equation

$$\frac{\partial C}{\partial t} = D\nabla^2 C, \tag{1}$$

where $C(\mathbf{x},t)$ is the density of agents, $D = (P/2d)\lim_{\Delta,\tau\to 0}(\Delta^2/\tau)$ is the diffusivity, and d is the physical dimension of the lattice.

Collective cell migration often involves situations with high cell densities and many cell-to-cell contacts [4,7–10]. Under these conditions crowding effects are often observed and have led to the development of *interacting* position-jump models to account for crowding [11]. These interacting position-jump models, also known as exclusion processes [12], allow each lattice site to be occupied by at most a single agent. In these interacting models the lattice spacing Δ is thought of as being equivalent to the cell diameter [13]. An interacting position-jump model is represented in the same way as a noninteracting position-jump model, except that individual movements now depend on the state of the system. For example, a motility event involving an agent attempting to step to an occupied target site would be aborted. These aborted motility events are thought to represent crowding effects in the system [13–15]. Interacting position-jump models have been used to represent many cell biology processes including cancer cell migration [15,16], wound healing [17,18], and embryonic development [4]. Extensions of the basic interacting position-jump model to deal with applications involving populations composed of distinct interacting subpopulations have also been described [11,19].

A population-level description of an interacting position-jump model can be derived from a discrete conservation statement in the limit that $\Delta \to 0$ and $\tau \to 0$ simultaneously. For unbiased transitions this process also leads to Eq. (1). The fact that noninteracting and interacting position-jump processes are governed by the same macroscopic description is counterintuitive, as we might expect that the differences in the random-walk model would be reflected in differences in the macroscopic model. However, simulation [11] and analysis [20] show that both unbiased interacting and unbiased noninteracting position-jump processes are in fact described by the linear diffusion equation.

Velocity-jump processes are a class of random walk in which each walker's velocity undergoes a series of discrete jumps [2,21–24]. Several authors have suggested that velocity-jump processes are better suited to represent collective biological motion than position-jump models [2,25]. Typically, a velocity-jump model involves simulating the movement of a population of agents on a regular lattice with lattice spacing Δ.

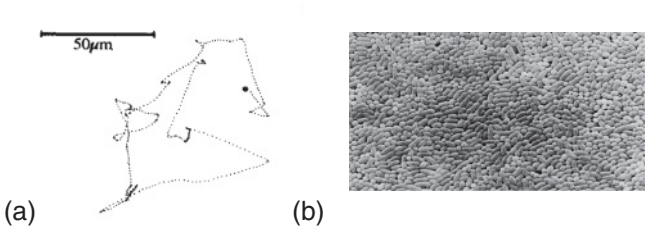

FIG. 1. (a) Three-dimensional trajectory of a single bacterium showing the stereotypical run and tumble motion characterized by many persistent runs at constant velocity and occasional tumbles corresponding to changes in velocity. (Reprinted from Ref. [6], with permission.) (b) Image of a crowded colony of *Escherichia coli*. (Reprinted from Ref. [26], with permission.)

During each discrete time interval, of duration τ, each agent undergoes a displacement of $\mathbf{v}\tau$ with probability $P \in [0,1]$. Here $\mathbf{v}$ is a velocity vector that encodes information about the speed and direction of motion for each agent. In addition to the possibility of changing position, during each discrete time interval of duration τ all agents are given the opportunity to change their velocity with probability $\lambda \in [0,1]$. When λ is zero we have perfectly persistent ballistic motion, with all agents continuing to move at a constant velocity. One of the key biological motivations behind velocity-jump models with $\lambda > 0$ is that they can capture the stereotypical "run and tumble" motion of isolated bacteria cells that undergo persistent motion with occasional changes in direction [1,6]. Figure 1(a) shows a three-dimensional trajectory of an isolated bacteria cell where we see that the motion is composed of many persistent "runs" with occasional "tumbles," which correspond to changes in velocity. Because the trajectory corresponds to an isolated bacteria cell, it is clear that crowding effects are unimportant for this particular system.

All velocity-jump models described in the literature are noninteracting. This means that crowding effects are ignored, multiple agents can reside on the same lattice site, and motility events that would require an agent to step across another agent are permitted. To describe a one-dimensional noninteracting velocity-jump process we consider a general one-dimensional lattice with lattice spacing Δ. During each time step of duration τ, all agents have the opportunity step a distance $\pm(v\tau)$ with probability $P \in [0,1]$. Here v is a dimensionless velocity, which we describe in detail in Sec. II. To account for differences in the direction of motion, the total population is considered as the sum of two subpopulations, with subpopulation L moving in the $-x$ direction and subpopulation R moving in the $+x$ direction. Turning events, whereby left-moving agents convert to right-moving agents and right-moving agents convert to left-moving agents, occur with probability λ during each time step. By constructing a discrete conservation statement for both subpopulations and taking the limit that $\Delta \to 0$ and $\tau \to 0$ simultaneously, we obtain [22,23]

$$\frac{\partial R}{\partial t} = -V\frac{\partial R}{\partial x} + \Lambda(L - R), \tag{2}$$

$$\frac{\partial L}{\partial t} = V\frac{\partial L}{\partial x} + \Lambda(R - L), \tag{3}$$

where $V = Pv\lim_{\Delta,\tau\to 0}(\Delta/\tau)$ is the advective velocity and $\Lambda = \lim_{\Delta,\tau\to 0}(\lambda/\tau)$ is the turning rate. In contrast with Eq. (1), where information propagates with infinite speed, we note that Eqs. (2) and (3) are a system of linear hyperbolic equations in which information propagates with finite speed. Instead of writing the macroscopic model as a system of two coupled equations, it is possible to define the total density as $S(x,t) = L(x,t) + R(x,t)$ and rewrite Eqs. (2) and (3) as a linear telegraph equation for $S(x,t)$ [2,22,23].

We note that until now there has been no corresponding theory developed for interacting analogs of the velocity-jump processes. Given that we are interested to use discrete random-walk models to describe systems with a high degree of cell-to-cell contact and crowding effects, the aim of this work is to formulate, derive, and validate several extensions of the traditional noninteracting velocity-jump process. For example, the colony of bacterial cells in Fig. 1(b) [26] shows that these kinds of cells can occur in densely crowded conditions. Although there is no experimental measurement of the individual trajectories of the bacterial cells in Fig. 1(b), we note that these cells are densely packed and we intuitively expect that the motion of individual cells in Fig. 1(b) will be reduced as a result of crowding effects that are not present in Fig. 1(a). In addition to the experimental image shown in Fig. 1(b), we note that other experimental systems have reported cell trajectory data that illustrate how cell motility is reduced by crowding effects. Such observations have been reported in several experimental systems including scratch assays with fibroblast cells [9] and the migration of embryonic precursor cells during development [10].

Although we have used the idea of collective cell migration to motivate our study, we believe that the models outlined in this work are also relevant to other biological transport processes. The motion of biomolecules along microtubules is a key process involved in maintaining proper cellular function [27]. Of particular relevance to the work outlined in this paper is the fact that the motion of biomolecules along microtubules is a one-dimensional process where crowding effects and ballistic motion can be important [28]. Therefore, the analysis outlined in our work will have application in the understanding of biological processes across a range of scales including collective motion of cells within tissues (such as wound healing and malignant invasion) as well as collective motion of biomolecules within a cell.

In addition to the random-walk models outlined so far, many other kinds of random-walk models are known to have application in studying biological and ecological motion. One area of great interest is the study of animal swarming behavior where alignment interactions [29] and group leader decisions [30] have been shown to be important for certain applications. It is also possible to study random-walk phenomena from the point of view of a continuous time random-walk framework instead of a discrete time framework [31].

This paper is outlined as follows. In Sec. II we summarize a traditional noninteracting one-dimensional velocity-jump process, derive the governing macroscopic equations, and explore the relationship between simulation data and the solution of the macroscopic equations. In Secs. III–V we propose three different cases of an interacting velocity-jump process. Each case builds on the previous case by introducing

more realistic, and more complex, forms of interaction. For each case we derive the corresponding macroscopic model and explore the relationship between discrete simulation data and the solution of the corresponding macroscopic models developed here. For our velocity-jump models with only one subpopulation and no turning, we provide an interpretation of the continuum models in Sec. VI. A discussion is presented in Sec. VII and we summarize in Sec. VIII.

II. CASE (0): NONINTERACTING VELOCITY-JUMP MODELS

To motivate our interacting velocity-jump models we first recall and present key results for the standard velocity-jump model. We do this for two reasons. First, it will be insightful to present our averaging arguments, simulation data, and discrete-continuum comparisons for the traditional noninteracting case before we present the more detailed interacting cases. Second, in this work we will compare discrete and continuum information in a way that is very different from previous studies. That is, we will develop continuum descriptions for the left-moving subpopulation $L(x,t)$ and the right-moving subpopulation $R(x,t)$ separately and then compare solutions of these continuum equations with the discrete data. In contrast, previous studies have considered developing models for the total population $S(x,t) = L(x,t) + R(x,t)$ only. We prefer to consider the subpopulation approach since we obtain more detailed information about the velocity-jump processes. Further, when we go on to consider interacting velocity-jump models, it is no longer mathematically convenient to rewrite the governing equations in terms of a single equation for $S(x,t)$.

A. Discrete simulation

To simulate a one-dimensional noninteracting velocity-jump process we consider a regular one-dimensional lattice with lattice spacing Δ. Each site is indexed $i \in \mathbb{Z}^+$ and the position of each site is $x = \Delta i$. Simulations will be updated by discretizing time into a series of discrete intervals of duration τ. The total duration of a simulation is given by $t = b\tau$, where b is the number of discrete time steps.

We will consider the population of agents to be composed of a left-moving subpopulation and a right-moving subpopulation, such as the schematic population shown in Fig. 2. In our simulations, if there is a total of N agents on the lattice, then during the next time step of duration τ, N agents are selected independently at random, one at a time. When chosen, an agent is then given the opportunity to change the direction of movement with probability $\lambda \in [0,1]$. Once the change in direction has been considered, the same agent is then given the opportunity to move with some probability $P \in [0,1]$. This means that right-moving agents will attempt to step in the $+x$ direction, while left-moving agents will attempt step in the $-x$ direction during that time step. After N agents have been chosen and given the opportunity to change direction and move, time is incremented by a duration τ.

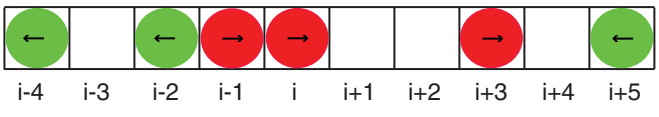

FIG. 2. (Color online) One-dimensional schematic used to illustrate the key differences between the traditional noninteracting velocity-jump process [case (0)] and the three interacting velocity-jump processes [cases (1)–(3)] introduced in this work. Light gray (green) agents are shown with a left arrow and dark gray (red) right-moving agents are shown with a right arrow.

All results presented in this paper have been produced by assessing changes in direction before motility events. For completeness, we also replicated all results by reversing the order of operations so that motility events were assessed before changes in direction. For all problems considered in this paper we observe that averaged simulation data do not depend on the order of operations in the discrete algorithm. This independence of the order of operations is similar to known results about operator splitting techniques that are used to generate numerical solutions of differential equations [32,33]. We note that some random-walk processes, in particular asymmetric processes, are sensitive to the order of update [34,35]; however, it appears that the models presented in this work are insensitive to these details.

Since we are considering a lattice-based velocity-jump process, our choice of parameters in the discrete simulations is restricted so that the displacement of each agent during any motility event is an integer multiple of the lattice spacing Δ. To describe this we set $v\tau = a\Delta$, where a is a positive integer with dimensions T/L. We note that there are several ways to interpret the scales in the problem and we choose to interpret v as a nondimensional measure of speed. Physically, v is a ratio of the number of lattice sites per computational step. We note that for the standard noninteracting model it is always possible to choose Δ and τ so that $v = 1$ and this corresponds to nearest-neighbor transitions on the scaled lattice. For the interacting cases introduced here, we take the most general approach and describe the random walk by specifying Δ, τ, and v separately without scaling. This allows us to consider non-nearest-neighbor transitions ($v > 1$). The details of the interacting cases outlined in Secs. III–V require that we retain the flexibility to study either nearest- or non-nearest-neighbor transitions. We achieve this by choosing v without any rescaling.

To demonstrate some key features of the velocity-jump process, we present three snapshots of a noninteracting velocity-jump process in Fig. 3. To initiate each simulation we occupy the ith lattice site with a left-moving agent with probability $L(x,0)$ or a right-moving agent with probability $R(x,0)$. Later in this work we will introduce crowding effects so that each lattice site can be occupied by at most a single agent. To be consistent with this approach we always deal with initial conditions that satisfy $L(x,0) + R(x,0) \leqslant 1$.

For all problems considered in this work we choose $L(x,0)$ to be Gaussian and $R(x,0)$ to be identically zero so that we have

$$R(x,0) = 0, \tag{4}$$

$$L(x,0) = w \exp\left[-\left(\frac{x - x_c}{q}\right)^2\right], \tag{5}$$

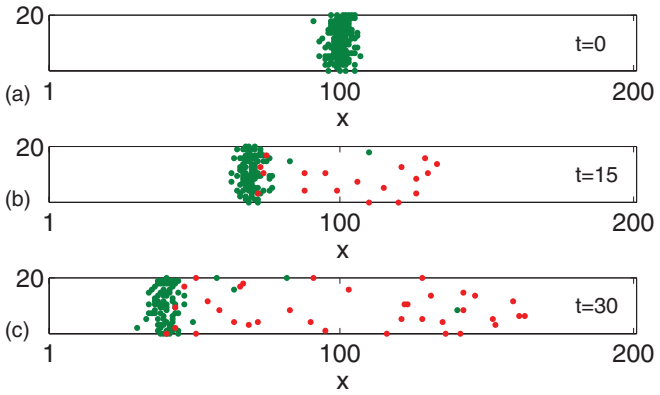

FIG. 3. (Color online) Snapshots of a one-dimensional noninteracting velocity-jump process. The distribution of agents in 20 identically prepared realizations are shown at (a) $t = 0$, (b) $t = 15$, and (c) $t = 30$. Each independent realization is presented as a separate row in (a)–(c). Each realization is performed on a one-dimensional lattice with $1 \leqslant x \leqslant 200$ and the parameters in the velocity-jump process are $\Delta = \tau = P = 1$ with $v = 2$ and $\lambda = 0.01$. Each snapshot shows light gray (green) left-moving agents and dark gray (red) right-moving agents. The initial distribution of agents is given by Eqs. (4) and (5) with $q = 4$, $w = 0.5$, and $x_c = 100$.

where $w \in (0,1]$ specifies, on average, the maximum density of agents per lattice site and q is a positive parameter specifying the average width of the Gaussian profile that is centered at x_c. To initiate a simulation we consider each lattice site at position x separately. A random number $U \in [0,1]$ is drawn from the uniform distribution. If $0 \leqslant U \leqslant L(x,0)$, we place a left-moving agent at that site, whereas if $L(x,0) < U \leqslant 1$, we leave that site unoccupied.

The algorithm was used to generate results shown in Fig. 3, where we show several snapshots, each of which are composed of 20 identically prepared realizations of the noninteracting velocity-jump process with $v = 2$ and $\lambda = 0.01$. By showing all 20 realizations side by side in Fig. 3, we aim to illustrate the stochastic nature of the algorithm since the distribution of agents in each row of the lattice in Figs. 3(a)–3(c) is quite different. The distribution of agents in Fig. 3 is consistent with our physical intuition about the noninteracting velocity-jump process. Given that we consider simulations with small λ, we expect that most of the initially left-moving subpopulation will continue move in the $-x$ direction at speed $v = 2$; the snapshots in Figs. 3(a)–3(c) confirm this expectation. As the simulation proceeds and t increases, we see that a small number of left-moving agents convert into right-moving agents. These right-moving agents then move in the $+x$ direction at speed $v = 2$. We note that in all simulation data presented in this work we always consider a sufficiently wide lattice and sufficiently short simulations that the agents on the lattice never touch the boundaries of the lattice during the time scale of the simulation.

To quantify the mean behavior of the velocity-jump process, we consider performing a large number of identically prepared realizations and average the occupancy of each lattice site across each realization. If R_i^m and L_i^m are the occupancy of right-moving and left-moving agents at site i during the mth realization, estimates of the mean agent densities are given by

$$\langle R_i \rangle = \frac{1}{M} \sum_{j=1}^{M} R_i^j, \tag{6}$$

$$\langle L_i \rangle = \frac{1}{M} \sum_{j=1}^{M} L_i^j, \tag{7}$$

where M is the number of identically prepared realizations used to construct the average. For all problems in this paper we choose M to be sufficiently large so that the density profiles of $\langle L_i \rangle$ and $\langle R_i \rangle$ are reasonably smooth and contain only modest fluctuations about the mean. At the same time we are also careful not to choose M too large otherwise the averaged profiles of $\langle L_i \rangle$ and $\langle R_i \rangle$ are so smooth that it will be difficult to visually distinguish the discrete density profiles from the corresponding continuum density profiles.

B. Macroscopic description

To develop a continuum partial differential equation (PDE) description of the noninteracting velocity-jump process we formulate a discrete conservation statement for both $\langle L_i \rangle$ and $\langle R_i \rangle$ and consider the change in average occupancy at site i during a discrete time step of duration τ. By considering all mechanisms in the discrete model we arrive at

$$\begin{aligned}\delta\langle R_i \rangle = {} & P\langle R_{i-v\tau} \rangle(1-\lambda) + P\langle L_{i-v\tau} \rangle(\lambda) + (1-P)\langle L_i \rangle(\lambda) \\ & - P\langle R_i \rangle(1-\lambda) - (1-P)\langle R_i \rangle(\lambda) - P\langle R_i \rangle(\lambda), \end{aligned} \tag{8}$$

$$\begin{aligned}\delta\langle L_i \rangle = {} & P\langle L_{i+v\tau} \rangle(1-\lambda) + P\langle R_{i+v\tau} \rangle(\lambda) + (1-P)\langle R_i \rangle(\lambda) \\ & - P\langle L_i \rangle(1-\lambda) - (1-P)\langle L_i \rangle(\lambda) - P\langle L_i \rangle(\lambda), \end{aligned} \tag{9}$$

where $\delta\langle L_i \rangle$ and $\delta\langle R_i \rangle$ represents the small change in the average occupancy of left-moving and right-moving agents at site i during the next time step of duration τ, respectively. These discrete conservation statements encode all the physical processes in the random-walk model and each term on the right-hand side has a simple physical interpretation. For example, on the right-hand side of Eq. (9) we have $P\langle L_{i+v\tau} \rangle(1-\lambda)$, the probability that a left-moving agent at site $i + v\tau$ does not change direction and moves into site i; $P\langle R_{i+v\tau} \rangle(\lambda)$, the probability that a right-moving agent at site $i + v\tau$ changes direction and moves into site i; $(1-P)\langle R_i \rangle(\lambda)$, the probability that a right-moving agent at site i changes direction and does not attempt to leave site i; $P\langle L_i \rangle(1-\lambda)$, the probability that a left-moving agent leaves site i and does not change direction; $(1-P)\langle L_i \rangle(\lambda)$, the probability that a left-moving agent at site i changes direction and does not attempt to leave site i; and $P\langle L_i \rangle(\lambda)$, the probability that a left-moving agent leaves site i and changes direction. We remark that the last two terms on the right-hand side of Eq. (9) can be summed to give $-P\langle L_i \rangle(\lambda) - (1-P)\langle L_i \rangle(\lambda) = -\langle L_i \rangle(\lambda)$. This simplified term can be interpreted as the probability that a left-moving agent at site i changes direction, regardless of whether or not it attempts to leave site i.

To convert Eqs. (8) and (9) into continuous macroscopic PDEs, we will identify the average densities $\langle L_i \rangle$ and $\langle R_i \rangle$,

with their continuous counterparts $L(x,t)$ and $R(x,t)$, and then expand all terms in a truncated Taylor series about site i as

$$R(i \pm a\Delta,t) = R(i,t) \pm (a\Delta)\frac{\partial R(i,t)}{\partial x} + O(a\Delta)^2, \quad (10)$$

$$L(i \pm a\Delta,t) = L(i,t) \pm (a\Delta)\frac{\partial L(i,t)}{\partial x} + O(a\Delta)^2. \quad (11)$$

We now substitute Eqs. (10) and (11) into the discrete conservation statements Eqs. (8) and (9). After dividing through by τ, we consider the limit as $\Delta \to 0$ and $\tau \to 0$ simultaneously and obtain

$$\frac{\partial R}{\partial t} = -V\frac{\partial R}{\partial x} + \Lambda(L - R), \quad (12)$$

$$\frac{\partial L}{\partial t} = V\frac{\partial L}{\partial x} + \Lambda(R - L), \quad (13)$$

$$V = Pv\lim_{\Delta,\tau\to 0}\left(\frac{\Delta}{\tau}\right), \quad \Lambda = \lim_{\Delta,\tau\to 0}\left(\frac{\lambda}{\tau}\right). \quad (14)$$

Equations (12) and (13) are a system of coupled linear hyperbolic PDEs. To ensure that the coefficients in the PDEs are finite we require that $\lambda = O(\tau)$ as $\Delta \to 0$ and $\tau \to 0$ jointly with the ratio Δ/τ held constant [2,31,36]. All discrete simulations performed in this work are for small finite values of Δ and τ; therefore, we expect that the continuum model will match the discrete model for small values of λ only [2,31,36]. We explore this effect in Sec. II C.

To make a continuum-discrete comparison we generate numerical solutions of Eqs. (12) and (13) on the same domain as the discrete simulations. We use no-flux boundary conditions at both boundaries for both subpopulations and apply the same initial conditions given by Eqs. (4) and (5). All PDE models in this work are solved using an upwind finite-difference approximation on a grid with constant grid spacing δx and implicit Euler stepping with constant time steps of duration δt [37]. The two PDE models are solved sequentially. Picard linearization, with tolerance ϵ, is used to solve the resulting algebraic systems [38].

We now illustrate how averaged discrete data compare with solutions of the corresponding continuum models in Fig. 4. In this case we consider a lattice with $1 \leqslant x \leqslant 2000$. One thousand identically prepared realizations of the discrete process were generated and average density profiles were obtained using Eqs. (6) and (7). Numerical solutions of Eqs. (12) and (13) were obtained for the same initial condition and boundary conditions. These numerical solutions are superimposed on the discrete density profiles in Fig. 4 for a range of λ values and this shows that the PDE models are able to accurately predict the mean density distribution.

C. Quality of continuum-discrete match

Although we have demonstrated excellent quality of the continuum-discrete match for a range of parameters in Fig. 4, our limiting analysis suggests that the quality of the continuum-discrete match will be parameter dependent. We will now briefly explore these effects. To ensure that the coefficients in Eqs. (12) and (13) are finite, we require that $\lambda = O(\tau)$ as $\Delta \to 0$ and $\tau \to 0$ jointly with the ratio Δ/τ held constant [2,31,36]. This implies that the continuum

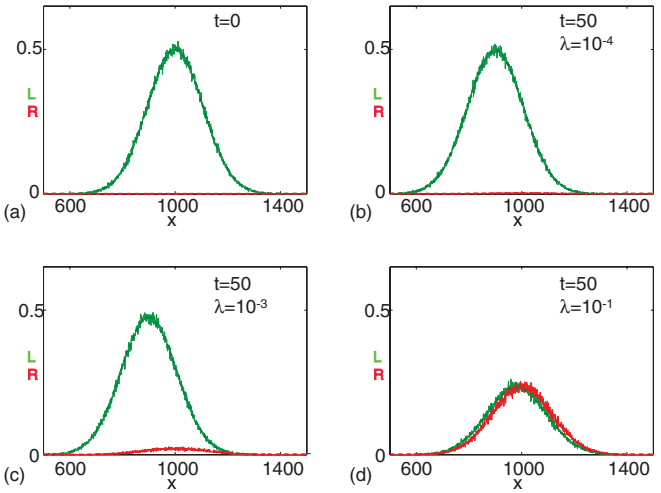

FIG. 4. (Color online) Comparison of discrete and continuum density profiles for various noninteracting velocity-jump processes with small turning rates. Simulations are performed on a one-dimensional lattice with $1 \leqslant x \leqslant 2000$ and the parameters in the velocity-jump process are $\Delta = \tau = P = 1$ with $v = 2$ and various values of λ. The initial distribution of agents is given by Eqs. (4) and (5) with $q = 150$, $w = 0.5$, and $x_c = 1000$. Density profiles from the discrete simulations are computed using Eqs. (6) and (7) with $M = 1000$ identically prepared realizations. The profile shown in (a) corresponds to the initial condition and the three profiles shown in (b)–(d) correspond to $\lambda = 10^{-4}, 10^{-3}$, and 10^{-1}, respectively. The stochastic density profiles are shown by the thin solid, dark gray (red) line and the thin solid, light gray (green) line for the left-moving and right-moving subpopulations, respectively. The solution of the continuum PDE model Eqs. (12) and (13) is shown by the superimposed, thick dashed, dark gray (red) line and the thick dashed, light gray (green) line for $L(x,t)$ and $R(x,t)$, respectively. The numerical solution of the PDE models was obtained using the technique outlined in the manuscript with $\delta x = 0.5$, $\delta t = 0.05$, and $\epsilon = 1 \times 10^{-6}$.

model will match the discrete model for small values of λ only [2,31,36]. To demonstrate this restriction we repeat the simulations shown in Fig. 4 for larger turning probabilities and present the continuum-discrete comparison in Figs. 5(a) and 5(b). Here we see that the solution of the continuum equations fails to match the discrete profiles and the discrepancy between the continuum and discrete profiles increases with λ. This divergence between the continuum and discrete profiles is consistent with our limiting analysis and is also consistent with previous analysis, which showed that the noninteracting velocity-jump process can be described by a parabolic equation in the limit that $\lambda \to \infty$ [39].

In addition to comparing continuum and discrete profiles for the two subpopulations in Figs. 5(a) and 5(b), we also compare continuum and discrete profiles for the total population $S(x,t) = L(x,t) + R(x,t)$ in Figs. 5(c) and 5(d). It is interesting to note that the total continuum density profile and the total discrete density profile match very well even for larger turning rates [Figs. 5(c) and 5(d)], whereas the continuum-discrete match for the two subpopulations is very poor [Figs. 5(a) and 5(b)]. This observation justifies our approach of focusing on conducting continuum-discrete comparisons for

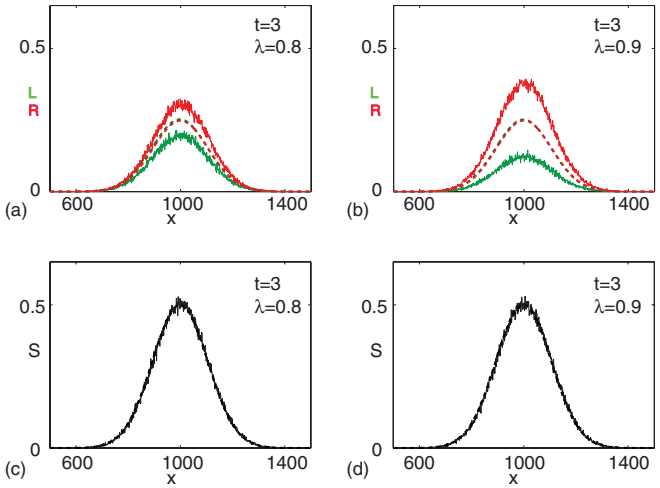

FIG. 5. (Color online) Comparison of discrete and continuum density profiles for various noninteracting velocity-jump processes with larger turning rates. Simulations are performed on a one-dimensional lattice with $1 \leqslant x \leqslant 2000$ and the parameters in the velocity-jump process are $\Delta = \tau = P = 1$ with $v = 2$ and various values of λ. The initial distribution of agents is given by Eqs. (4) and (5) with $q = 150$, $w = 0.5$, and $x_c = 1000$. Density profiles from the discrete simulations are computed using Eqs. (6) and (7) with $M = 2000$ identically prepared realizations and the profiles shown in (a) and (b) correspond to $\lambda = 0.8$ and 0.9, respectively. The stochastic density profiles are shown by the thin solid, dark gray (red) line and the thin solid, light gray (green) line for the left-moving and right-moving subpopulations, respectively. The solution of the continuum PDE model Eqs. (12) and (13) is shown by the superimposed, thick dashed, dark gray (red) line and the thick dashed, light gray (green) line for $L(x,t)$ and $R(x,t)$, respectively. Results in (c) and (d) are for the total population $S(x,t) = L(x,t) + R(x,t)$ and these profiles were obtained by summing the corresponding profiles in (a) and (b) with the discrete results shown by the thin solid line and the continuum results shown by the thick dotted line. The numerical solution of the PDE models was obtained using the technique outlined in the paper with $\delta x = 0.5$, $\delta t = 0.05$, and $\epsilon = 1 \times 10^{-6}$.

the subpopulations instead of the total population. Our results in Fig. 5 show that it is more rigorous to compare results for the subpopulations separately. One reason for this is that the expression for the total population $S(x,t) = L(x,t) + R(x,t)$ is underdetermined and there are infinitely many choices of $L(x,t)$ and $R(x,t)$ that can be added to give the correct profile for $S(x,t)$, as we have demonstrated in Fig. 5.

We remark that all continuum-discrete matches presented in this paper correspond to the initial condition given by Eqs. (4) and (5) with $P = 1$. These choices correspond to situations where we consider an initially Gaussian distribution of left-moving agents and that every agent always moves within each computational time step. We also generated and compared discrete and continuum density profiles for a range of other initial conditions (e.g., Heaviside functions and multiple Gaussian distributions) for situations that involved both subpopulations present on the lattice at $t = 0$, so that $L(x,0) > 0$ and $R(x,0) > 0$ simultaneously. Furthermore, we also generated and compared discrete and continuum density profiles for other situations where $P < 1$, which corresponds to the situation where agents need not move in every single time step. Our physical interpretation of setting $P < 1$ is that an agent is able to rest during some time steps. For all these additional situations we observed the exact same trends as we demonstrate here in Fig. 4. Instead of presenting results for all possible initial conditions and parameter combinations, we chose to present all results in this work using Eqs. (4) and (5) and $P = 1$ since these conditions are sufficient for us to clearly demonstrate the key features of our study.

Now that we have demonstrated how the noninteracting discrete density profiles compare with solution of the governing PDE models, we will systematically introduce three different ways to represent crowding effects into the velocity-jump process. In each case we will perform simulations, derive the relevant governing PDE models, and compare the continuum and discrete density profiles. From this point forward we will consider sufficiently small values of the turning probability λ so that we expect a good match between the continuum and discrete profiles.

III. CASE (1): AGENTS MOVE TO THE TARGET SITE ONLY IF THE TARGET SITE IS VACANT

In the first instance we will introduce the most straightforward form of agent-to-agent interaction by preventing multiple agents from residing on the same lattice site. This is achieved by performing simulations in the exact same way as we did for the noninteracting problem, except that potential motility events that would place more than one agent on any target site are aborted. In essence, this extension means that we are transforming a traditional noninteracting velocity-jump process into an exclusion process [12]. For biological applications, we interpret the lattice spacing as being the same length as the cell diameter [13].

To understand the details of the interaction, consider the configuration shown in Fig. 2 for a system in which $v\tau = 2\Delta$. Under noninteracting conditions [case (0)], the left-moving agent residing at site $i - 2$ would attempt to step to site $i - 4$ (with probability P), meaning that two agents could reside at site $i - 4$ simultaneously. However, for the interacting velocity-jump model developed in this section [case (1)], such a move would be aborted. Similarly, for case (1) the right-moving agent at site $i - 1$ would be permitted to step to the site $i + 1$ since the target site is vacant, whereas the left-moving agent at site $i + 5$ would not be permitted to step to site $i + 3$.

To demonstrate the effects of this interaction mechanism we present a snapshot of 20 identically prepared realizations in Figs. 6(a)–6(c). Figure 6(a) shows an initial distribution of left-moving agents. Figure 6(b) shows 20 identically prepared realizations of a noninteracting velocity-jump process [case (0)], whereas Fig. 6(c) shows 20 identically prepared realizations of the interacting velocity-jump process [case (1)], both with $v = 2$ and $\lambda = 0.01$. Comparing the snapshots in Figs. 6(b) and 6(c) shows that the distribution of left-moving agents appears to be further spread out in the interacting case relative to the noninteracting case.

To understand these differences we will incorporate the crowding effects into the discrete conservation statements that

are given by

$$\begin{aligned}\delta\langle R_i\rangle = {} & P\langle R_{i-v\tau}\rangle(1-\langle L_i\rangle-\langle R_i\rangle)(1-\lambda)+P\langle L_{i-v\tau}\rangle(1-\langle L_i\rangle-\langle R_i\rangle)(\lambda)+P\langle L_i\rangle(\langle L_{i+v\tau}\rangle+\langle R_{i+v\tau}\rangle)(\lambda)\\ & +(1-P)\langle L_i\rangle(\lambda)-P\langle R_i\rangle(1-\langle L_{i+v\tau}\rangle-\langle R_{i+v\tau}\rangle)(1-\lambda)-P\langle R_i\rangle(1-\langle L_{i-v\tau}\rangle-\langle R_{i-v\tau}\rangle)(\lambda)\\ & -P\langle R_i\rangle(\langle L_{i-v\tau}\rangle+\langle R_{i-v\tau}\rangle)(\lambda)-(1-P)\langle R_i\rangle(\lambda), \qquad (15)\\ \delta\langle L_i\rangle = {} & P\langle L_{i+v\tau}\rangle(1-\langle L_i\rangle-\langle R_i\rangle)(1-\lambda)+P\langle R_{i+v\tau}\rangle(1-\langle L_i\rangle-\langle R_i\rangle)(\lambda)+P\langle R_i\rangle(\langle L_{i-v\tau}\rangle+\langle R_{i-v\tau}\rangle)(\lambda)\\ & +(1-P)\langle R_i\rangle(\lambda)-P\langle L_i\rangle(1-\langle L_{i-v\tau}\rangle-\langle R_{i-v\tau}\rangle)(1-\lambda)-P\langle L_i\rangle(1-\langle L_{i+v\tau}\rangle-\langle R_{i+v\tau}\rangle)(\lambda)\\ & -P\langle L_i\rangle(\langle L_{i+v\tau}\rangle+\langle R_{i+v\tau}\rangle)(\lambda)-(1-P)\langle L_i\rangle(\lambda). \qquad (16)\end{aligned}$$

We remark that the last three terms on the right-hand side of Eq. (16) can be added to give $-\langle L_i\rangle(\lambda)$, which can be interpreted as the probability that a left-moving agent at site i changes direction. Each of the terms in Eqs. (15) and (16) has a straightforward physical interpretation. For example, the terms in Eq. (16) correspond to $P\langle L_{i+v\tau}\rangle(1-\langle L_i\rangle-\langle R_i\rangle)(1-\lambda)$, the probability that a left-moving agent at site $i+v\tau$ attempts to move, does not change direction, and that the target site, site i, is vacant; $P\langle R_{i+v\tau}\rangle(1-\langle L_i\rangle-\langle R_i\rangle)(\lambda)$, the probability that a right-moving agent at site $i+v\tau$ attempts to move, changes direction, and that site i is vacant; $P\langle R_i\rangle(\langle L_{i-v\tau}\rangle+\langle R_{i-v\tau}\rangle)(\lambda)$, the probability that a right-moving agent at site i attempts to move, changes direction, and that the target site, site $i-v\tau$, is occupied; $(1-P)\langle R_i\rangle(\lambda)$, the probability that a right-moving agent at site i does not attempt to move and changes direction; $P\langle L_i\rangle(1-\langle L_{i-v\tau}\rangle-\langle R_{i-v\tau}\rangle)(1-\lambda)$, the probability that a left-moving agent at site i attempts to move, does not change direction, and that the target site, site $i-v\tau$, is vacant; $P\langle L_i\rangle(1-\langle L_{i+v\tau}\rangle-\langle R_{i+v\tau}\rangle)(\lambda)$, the probability that a left-moving agent at site i attempts to move, changes direction, and that the target site, site $i+v\tau$, is vacant; $P\langle L_i\rangle(\langle L_{i+v\tau}\rangle+\langle R_{i+v\tau}\rangle)(\lambda)$, the probability that a left-moving agent at site i attempts to move, changes direction, and that the target site, site $i+v\tau$, is occupied; and $(1-P)\langle L_i\rangle(\lambda)$, the probability that a left-moving agent at site i does not attempt to move and changes direction. The key difference between Eqs. (15) and (16) and the noninteracting conservation equations (8) and (9) is the presence of factors such as $1-\langle L_i\rangle-\langle R_i\rangle$ in the terms that represent motility events. For example, the first term on the right-hand side of Eq. (16) represents a left-moving agent at site $i+\tau v$ that attempts to step to site i. This motility event will be successful only if site i is vacant; this condition is specified by introducing the factor $1-\langle L_i\rangle-\langle R_i\rangle$, which is the probability that site i is vacant. These additional factors ensure that all potential motility events would only take place provided the target site is vacant [11].

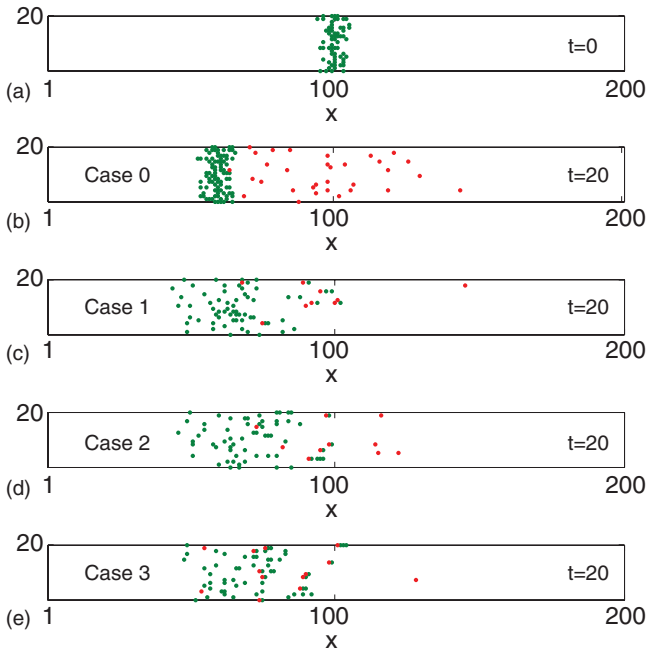

FIG. 6. (Color online) Snapshots of several one-dimensional noninteracting and interacting velocity-jump processes. The distribution of agents in 20 identically prepared realizations are shown at (a) $t=0$ and in (b)–(e) at $t=20$ for a range of interacting and noninteracting cases. Noninteracting results are shown in (b) while interacting cases (1)–(3) are shown in (c)–(e), respectively. Each independent realization is presented as a separate row in (a)–(e). All simulations are performed on a one-dimensional lattice with $1\leqslant x\leqslant 200$ and the parameters $\Delta=\tau=P=1$ with $v=2$ and $\lambda=0.01$. Each snapshot shows light gray (green) left-moving agents and dark gray (red) right-moving agents. The initial distribution of agents is given by Eqs. (4) and (5) with $q=4$, $w=0.5$, and $x_c=100$.

To understand how these changes affect the resulting PDE models, we substitute the truncated Taylor series expansions into Eqs. (15) and (16) and then divide through by τ. Considering the limit as $\Delta\to 0$ and $\tau\to 0$ simultaneously, we obtain

$$\frac{\partial R}{\partial t}=-V\frac{\partial}{\partial x}(R[1-R-L])+\Lambda(L-R), \qquad (17)$$

$$\frac{\partial L}{\partial t}=V\frac{\partial}{\partial x}(L[1-R-L])+\Lambda(R-L), \qquad (18)$$

$$V=Pv\lim_{\Delta,\tau\to 0}\left(\frac{\Delta}{\tau}\right),\quad \Lambda=\lim_{\Delta,\tau\to 0}\left(\frac{\lambda}{\tau}\right). \qquad (19)$$

Equations (17) and (18) are a system of coupled nonlinear hyperbolic PDEs. The presence of the $[1-L-R]$ factor in the flux terms in Eqs. (17) and (18) indicates that the flux of agents is zero in regions where space is completely occupied and $L(x,t)+R(x,t)=1$.

It is interesting to note that we have demonstrated that a noninteracting velocity-jump model and an interacting velocity-jump model give rise to very different continuum PDE representations. This is, in some sense, an expected result since it is intuitive to think that the differences in the random walk would give rise to differences in the PDE representations. However, as we have already outlined in Sec. I, it is well known that unbiased interacting position-jump

models and unbiased noninteracting position-jump models are both described by the same PDE model [11]. One way to interpret these differences between velocity-jump and position-jump models is that position-jump models are relatively insensitive to crowing effects, whereas velocity-jump models are relatively sensitive to crowding effects. This difference also suggests that velocity-jump models are, in some sense, better suited to interpreting collective cell migration problems rather than position-jump models since crowding effects are often observed in experimental cell migration studies [8–10].

To examine how the solution of Eqs. (17) and (18) compare with discrete density profiles we performed a large number of identically prepared realizations and extracted density profiles, which are shown in Figs. 7 and 8 with $\lambda = 0$ and 0.01, respectively. The solutions of the corresponding PDE models Eqs. (17) and (18) were generated with parameters, boundary conditions, and initial conditions to match the discrete simulations. Both the discrete and continuum density profiles are superimposed in Figs. 7–8(a) and Figs. 7–8(d). In all cases we see that the quality of the match between the continuum and discrete density profiles is excellent.

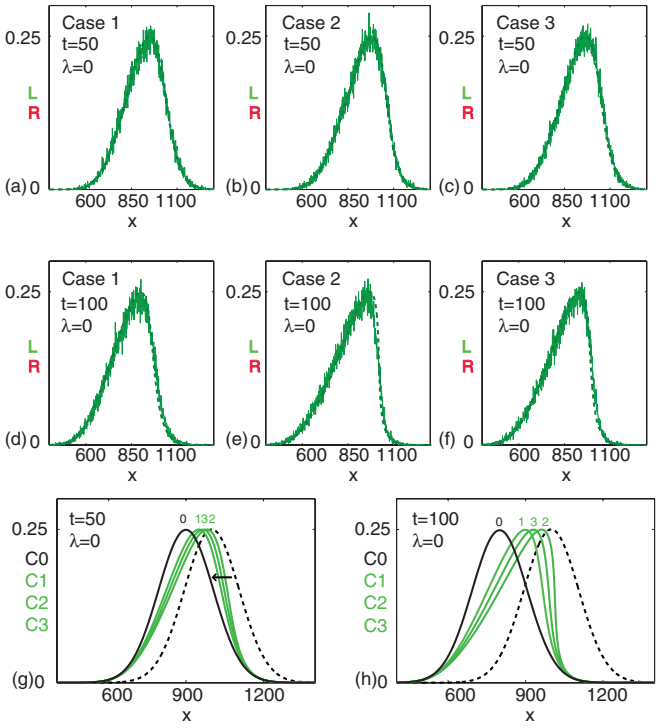

FIG. 7. (Color online) Comparison of discrete and continuum density profiles for various interacting velocity-jump processes with no turning $\lambda = 0$. Simulations are performed on a one-dimensional lattice with $1 \leqslant x \leqslant 2000$ and the parameters $\Delta = \tau = P = 1$ with $v = 2$. In all cases the initial distribution of agents is given by Eqs. (4) and (5) with $q = 150$, $w = 0.25$, and $x_c = 1000$. Density profiles from the discrete simulations are computed using Eqs. (6) and (7) with $M = 1000$ identically prepared realizations. The profiles in (a) and (d) are for case (1) at $t = 50$ and 100, respectively. The profiles in (b) and (e) are for case (2) at $t = 50$ and 100, respectively. The profiles in (c) and (f) are for case (3) at $t = 50$ and 100, respectively. The discrete profiles for the left-moving subpopulations are shown by the thin light gray (green) line. The solution of the continuum PDE models (Eqs. (17), (18), (22), (23), (27), and (28) are by the superimposed, thick dashed, light gray (green) line for $L(x,t)$. (g) and (h) Comparison of the continuum initial condition (dotted black line) with the solution of the noninteracting (solid black line) model and the three interacting models [light gray (green) solid line] for this particular problem at $t = 50$ and 100, respectively. The profiles for cases (0)–(3) are shown with the number indicating the case. The numerical solution of the PDE models was obtained using the technique outlined in the paper with $\delta x = 0.5$, $\delta t = 0.05$, and $\epsilon = 1 \times 10^{-6}$.

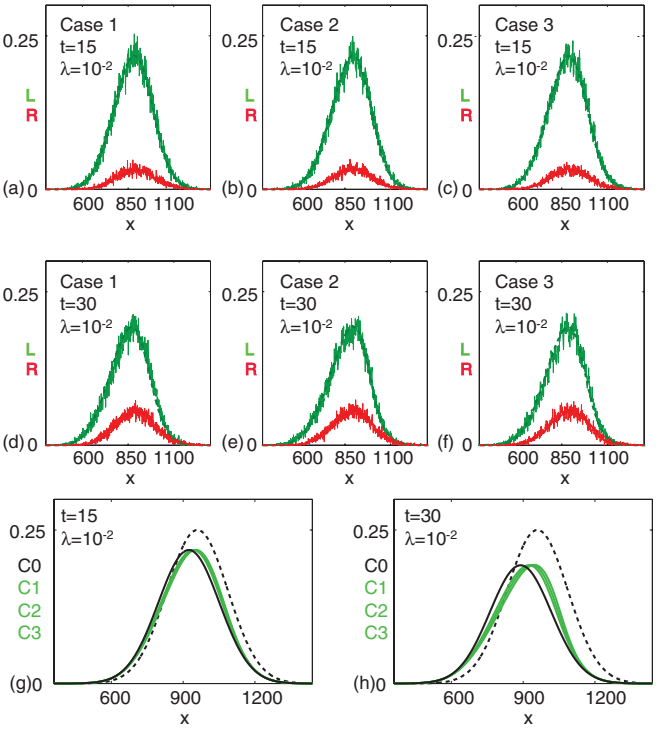

FIG. 8. (Color online) Comparison of discrete and continuum density profiles for various interacting velocity-jump processes with a small turning probability $\lambda = 0.01$. Simulations are performed on a one-dimensional lattice with $1 \leqslant x \leqslant 2000$ and the parameters $\Delta = \tau = P = 1$ with $v = 2$. In all cases the initial distribution of agents is given by Eqs. (4) and (5) with $q = 150$, $w = 0.25$, and $x_c = 1000$. Density profiles from the discrete simulations are computed using Eqs. (6) and (7) with $M = 1000$ identically prepared realizations. The profiles in (a) and (d) are for case (1) at $t = 15$ and 30, respectively. The profiles in (b) and (e) are for case (2) at $t = 15$ and 30, respectively. The profiles in (c) and (f) are for case (3) at $t = 15$ and 30, respectively. The stochastic density profiles for the left-moving subpopulations and the right-moving subpopulations are shown by the thin light gray (green) and dark gray (red) lines, respectively. The solutions of the continuum PDE models Eqs. (17), (18), (22), (23), (27), and (28) are shown by the superimposed, thick dashed, light gray (green) line for $L(x,t)$ and the thick dashed, dark gray (red) line for $R(x,t)$. (g) and (h) Comparison of the continuum initial condition (dotted black) with the solution of the noninteracting model (black line) and the three interacting models [light gray (green) line] for this particular problem at $t = 15$ and 30, respectively. The profiles of the left-moving subpopulation are shown for cases (0)–(3) with the number indicating the case. The numerical solution of the PDE models was obtained using the technique outlined in the paper with $\delta x = 0.5$, $\delta t = 0.05$, and $\epsilon = 1 \times 10^{-6}$.

We will now extend case (1) by considering a second form of agent-to-agent crowding. Interacting case (1) was derived to prevent motility events that would place multiple agents on a single site, but did not account for crowding effects that might take place during the displacement of an agent from one lattice site to another.

IV. CASE (2): AGENTS MOVE TO THE TARGET SITE ONLY IF THE TARGET SITE AND THE INTERMEDIATE SITES ARE VACANT

We will now introduce a second form of agent-to-agent interaction to prevent agents stepping across other agents during potential motility events. For example, in Fig. 2 with $v\tau = 2\Delta$, the agent residing at site $i-1$ would attempt to step to site $i+1$. Under the conditions described previously in Sec. III for case (1), this motility event would be permitted since the target site is vacant. For the distribution of agents shown in Fig. 2, this potential motility event seems to be unnatural since there is an agent residing at site i that would interfere with the transition of the original agent from site $i-1$ to the target site $i+1$. To account for this situation, in case (2) we will only permit motility events provided two conditions are met. First, the target site must be vacant. Second, all sites between the original site and the target site must be vacant.

These conditions can be translated into a set of discrete conservation statements that are given by

$$\delta\langle R_i\rangle = P\langle R_{i-v\tau}\rangle(1-\lambda)\prod_{s=0}^{v\tau-1}(1-\langle L_{i-s}\rangle-\langle R_{i-s}\rangle)+P\langle L_{i-v\tau}\rangle(\lambda)\prod_{s=0}^{v\tau-1}(1-\langle L_{i-s}\rangle-\langle R_{i-s}\rangle)$$
$$+P\langle L_i\rangle(\lambda)\left[1-\prod_{s=1}^{v\tau}(1-\langle L_{i+s}\rangle-\langle R_{i+s}\rangle)\right]+(1-P)\langle L_i\rangle(\lambda)-P\langle R_i\rangle(1-\lambda)\prod_{s=1}^{v\tau}(1-\langle L_{i+s}\rangle-\langle R_{i+s}\rangle)-(\lambda)\langle R_i\rangle, \tag{20}$$

$$\delta\langle L_i\rangle = P\langle L_{i+v\tau}\rangle(1-\lambda)\prod_{s=0}^{v\tau-1}(1-\langle L_{i+s}\rangle-\langle R_{i+s}\rangle)+P\langle R_{i+v\tau}\rangle(\lambda)\prod_{s=0}^{v\tau-1}(1-\langle L_{i+s}\rangle-\langle R_{i+s}\rangle)$$
$$+P\langle R_i\rangle(\lambda)\left[1-\prod_{s=1}^{v\tau}(1-\langle L_{i-s}\rangle-\langle R_{i-s}\rangle)\right]+(1-P)\langle R_i\rangle(\lambda)-P\langle L_i\rangle(1-\lambda)\prod_{s=1}^{v\tau}(1-\langle L_{i-s}\rangle-\langle R_{i-s}\rangle)-(\lambda)\langle L_i\rangle. \tag{21}$$

The key difference between Eqs. (20) and (21) and the discrete conservation statements in Sec. III for case (1) [Eqs. (15) and (16)] is that now we have products of terms such as $\prod_{s=0}^{v\tau-1}(1-\langle L_{i+s}\rangle-\langle R_{i+s}\rangle)$ appearing in the discrete conservation statement. These product terms reflect the fact that successful motility events require not just one vacant site, but now require a string of adjacent sites to be vacant for the motility event to be successful. To examine the continuum limit of Eqs. (20) and (21) we substitute the truncated Taylor series expansions into the discrete conservation statements. Dividing through by τ and considering the limit as $\Delta\to 0$ and $\tau\to 0$ simultaneously, we obtain

$$\frac{\partial R}{\partial t} = -V\frac{\partial}{\partial x}\left(R[1-R-L]^v\right)+\Lambda(L-R), \tag{22}$$

$$\frac{\partial L}{\partial t} = V\frac{\partial}{\partial x}\left(L[1-R-L]^v\right)+\Lambda(R-L), \tag{23}$$

$$V = Pv\lim_{\Delta,\tau\to 0}\left(\frac{\Delta}{\tau}\right),\quad \Lambda = \lim_{\Delta,\tau\to 0}\left(\frac{\lambda}{\tau}\right). \tag{24}$$

Equations (22) and (23) are a system of coupled nonlinear hyperbolic PDEs, with the $[1-L-R]^v$ factor in the flux terms indicating that the flux of agents is zero in regions where space is completely occupied and $L(x,t)+R(x,t)=1$. For the simplest case with $v=1$, Eqs. (22) and (23) for case (2) are identical to Eqs. (17) and (18) for case (1). For $v>1$ the crowding factor $[1-L-R]^v$ in the flux terms for case (2) [Eqs. (22) and (23)] is smaller than the crowding factor $[1-L-R]$ in the flux terms for case (1) [Eqs. (17) and (18)], implying that the crowding effects for case (2) will act to reduce the population-level motility to a greater extent than case (1) whenever $v>1$.

To examine how the solution of Eqs. (22) and (23) compare with discrete density profiles we performed a large number of identically prepared realizations and extracted density profiles, which are shown in Figs. 7 and 8 with $\lambda=0$ and 0.01, respectively. The solutions of the corresponding PDE models Eqs. (22) and (23) were generated with parameters, boundary conditions, and initial conditions to match the discrete simulations. The discrete and continuum density profiles are superimposed in Figs. 7(b) and 8(b) and Figs. 7(e) and 8(e), where again we see that the quality of the match between the discrete and continuum profiles is excellent.

V. CASE (3): AGENTS MOVE TO THE TARGET OR AS FAR AS POSSIBLE TOWARD THE TARGET SITE UNTIL ANOTHER AGENT BLOCKS THE PATH

We will now extend cases (1) and (2) by considering a third and final form of agent-to-agent crowding. If we consider the distribution of agents in Fig. 2 for the case in which $v\tau = 2\Delta$,

then the left-moving agent at site $i+5$ would attempt to move to site $i+3$, which is already occupied by a right-moving agent. For interaction cases (1) and (2) this potential movement event would be aborted because the target site and/or the sites across which the agent would move to reach the target site are occupied. Instead of strictly imposing that all sites between the original site and the target site must be vacant to allow a motility event to take place, we will now introduce the most complex form of interaction whereby an agent will attempt to step to a target site and will only move as far as it can until either it (i) reaches the target site without stepping on or stepping across another agent or (ii) meets another agent obstructing its path to the target site. For (ii) the motile agent then steps as far along the path as possible without stepping through any obstructing agent. For example, in Fig. 2 with $v\tau = 2\Delta$, the left-moving agent at site $i+5$ would attempt to step to site $i+3$ and in doing so will move left until it becomes obstructed by the agent residing at site $i+3$, causing the motile agent to be deposited at site $i+4$. In summary, for case (3) we will allow an agent to move as far as it can until the motility event is blocked by any other agent lying in the path of the motile agent.

This mechanism can be translated into a set of discrete conservation statements given by

$$\begin{aligned}\delta\langle R_i\rangle &= P\langle R_{i-v\tau}\rangle(1-\lambda)\prod_{s=0}^{v\tau-1}(1-\langle L_{i-s}\rangle-\langle R_{i-s}\rangle)+P\langle L_{i-v\tau}\rangle(\lambda)\prod_{s=0}^{v\tau-1}(1-\langle L_{i-s}\rangle-\langle R_{i-s}\rangle)\\&+P(\lambda)\sum_{s=1}^{v\tau-1}\left[\langle L_{i-s}\rangle(\langle L_{i+1}\rangle+\langle R_{i+1}\rangle)\prod_{n=0}^{s-1}(1-\langle L_{i-n}\rangle-\langle R_{i-n}\rangle)\right]\\&+P(1-\lambda)\sum_{s=1}^{v\tau-1}\left[\langle R_{i-s}\rangle(\langle L_{i+1}\rangle+\langle R_{i+1}\rangle)\prod_{n=0}^{s-1}(1-\langle L_{i-n}\rangle-\langle R_{i-n}\rangle)\right]\\&+P(\lambda)\langle L_i\rangle(\langle L_{i+1}\rangle+\langle R_{i+1}\rangle)+(1-P)\langle L_i\rangle(\lambda)-P(1-\lambda)\langle R_i\rangle(1-\langle L_{i+1}\rangle-\langle R_{i+1}\rangle)-\langle R_i\rangle(\lambda),\end{aligned}\tag{25}$$

$$\begin{aligned}\delta\langle L_i\rangle &= P\langle L_{i+v\tau}\rangle(1-\lambda)\prod_{s=0}^{v\tau-1}(1-\langle L_{i+s}\rangle-\langle R_{i+s}\rangle)+P\langle R_{i+v\tau}\rangle(\lambda)\prod_{s=0}^{v\tau-1}(1-\langle L_{i+s}\rangle-\langle R_{i+s}\rangle)\\&+P(\lambda)\sum_{s=1}^{v\tau-1}\left[\langle R_{i+s}\rangle(\langle L_{i-1}\rangle+\langle R_{i-1}\rangle)\prod_{n=0}^{s-1}(1-\langle L_{i+n}\rangle-\langle R_{i+n}\rangle)\right]\\&+P(1-\lambda)\sum_{s=1}^{v\tau-1}\left[\langle L_{i+s}\rangle(\langle L_{i-1}\rangle+\langle R_{i-1}\rangle)\prod_{n=0}^{s-1}(1-\langle L_{i+n}\rangle-\langle R_{i+n}\rangle)\right]\\&+P(\lambda)\langle R_i\rangle(\langle L_{i-1}\rangle+\langle R_{i-1}\rangle)+(1-P)\langle R_i\rangle(\lambda)-P(1-\lambda)\langle L_i\rangle(1-\langle L_{i-1}\rangle-\langle R_{i-1}\rangle)-\langle L_i\rangle(\lambda).\end{aligned}\tag{26}$$

We now substitute the truncated Taylor series expansions into the discrete conservation statements and divide through by τ. Considering the limit as $\Delta\to 0$ and $\tau\to 0$ simultaneously, we obtain

$$\frac{\partial R}{\partial t} = -V\frac{\partial}{\partial x}\left\{R\left[1+\sum_{n=1}^{v}\left(\frac{(-1)^n(v+1)!(L+R)^n}{v(n+1)!(v-n)!}\right)\right]\right\}+\Lambda(L-R),\tag{27}$$

$$\frac{\partial L}{\partial t} = V\frac{\partial}{\partial x}\left\{L\left[1+\sum_{n=1}^{v}\left(\frac{(-1)^n(v+1)!(L+R)^n}{v(n+1)!(v-n)!}\right)\right]\right\}+\Lambda(R-L),\tag{28}$$

$$V = Pv\lim_{\Delta,\tau\to 0}\left(\frac{\Delta}{\tau}\right),\quad \Lambda = \lim_{\Delta,\tau\to 0}\left(\frac{\lambda}{\tau}\right).\tag{29}$$

Equations (27) and (28) are a system of coupled nonlinear hyperbolic PDEs with very complicated crowding factors in the flux terms.

To see the relationship between Eqs. (27) and (28) and the previous systems of PDEs for cases (0)–(2), we can rewrite the summation terms that appear in the flux terms to arrive at

$$\frac{\partial R}{\partial t} = -V\frac{\partial}{\partial x}\left\{R\left[(1-R-L)\left(\frac{1-(1-R-L)^v}{v(R+L)}\right)\right]\right\}+\Lambda(L-R),\tag{30}$$

$$\frac{\partial L}{\partial t} = V\frac{\partial}{\partial x}\left\{L\left[(1-R-L)\left(\frac{1-(1-R-L)^v}{v(R+L)}\right)\right]\right\}+\Lambda(R-L),\tag{31}$$

$$V = Pv\lim_{\Delta,\tau\to 0}\left(\frac{\Delta}{\tau}\right),\quad \Lambda = \lim_{\Delta,\tau\to 0}\left(\frac{\lambda}{\tau}\right).\tag{32}$$

Written in this form, we can see that Eqs. (30) and (31) are related to the previous PDE models. For example, by setting $v=1$, it is clear that the PDE models for case (1) [Eqs. (17) and (18)], case (2) [Eqs. (22) and (23)], and case (3) [Eqs. (30) and (31)] all relax to become the same expression.

To examine how the solution of Eqs. (27) and (28) compares with discrete density profiles we performed a large number of identically prepared realizations and extracted density profiles, which are shown in Figs. 7 and 8 with $\lambda = 0$ and 0.01,

respectively. The solutions of the corresponding PDE models Eqs. (27) and (28) were generated with the same parameters, boundary conditions, and initial condition to match the discrete simulations. The discrete and continuum density profiles are superimposed in Figs. 7(c) and 8(c) and Figs. 7(f) and 8(f), respectively, where again we see that the quality of match between the discrete and continuum profiles is excellent.

It is now relevant to mention some key differences between the traditional noninteracting case and the interacting cases with respect to scaling. In the noninteracting case it is always possible to scale our choice of Δ and τ in the random-walk model so that $v = 1$. This amounts to considering nearest-neighbor transitions on the rescaled lattice. Conversely, for the interacting cases we wish to study crowding effects and it is relevant to consider situations where these crowding effects might occur as an agent attempts to step across many lattice sites so that $v > 1$. Therefore, for the interacting cases, we must be able to choose Δ, τ, and v independently without rescaling.

VI. ZERO TURNING RATE $\Lambda = 0$

The nonlinearity in the PDE models for cases (1)–(3) is most easily illustrated in Fig. 7, which is for $\Lambda = 0$ (zero turning rate). With the initial conditions given by Eqs. (4) and (5), setting $\Lambda = 0$ means that $R \equiv 0$ for all time, leaving only left-moving agents $L > 0$. Under these conditions we have

$$\frac{\partial L}{\partial t} = -\frac{\partial J}{\partial x}, \tag{33}$$

where, with the further assumption that $\Delta = \tau = P = 1$ (as in Fig. 7), we find that the flux J is

$$J = J_0 = -vL \quad \text{[case (0)]}, \tag{34}$$

$$J = J_1 = -vL(1-L) \quad \text{[case (1)]}, \tag{35}$$

$$J = J_2 = -vL(1-L)^v \quad \text{[case (2)]}, \tag{36}$$

$$J = J_3 = -(1-L)[1-(1-L)^v] \quad \text{[case (3)]}. \tag{37}$$

In regions for which $L \ll 1$ the density of agents is low and intuitively we would expect each of the cases (1)–(3) to behave like case (0), as vacant sites are plentiful, and any attempted movement is likely to be successful. Indeed, each $J_m \sim -vL$ as $L \to 0^+$ for $m = 1,2,3$, agreeing with case (0) ($J_0 = -vL$) in the dilute limit. In contrast, in regions for which $1 - L \ll 1$ the density of agents is high and crowding effects are most important. In densely populated regions we expect (for $v \geqslant 2$) that $|J_1|$ is larger than $|J_3|$ and that $|J_3|$ is much larger than $|J_2|$ since in a crowded region agents are more likely to move under the case (1) scenario, with the only test being whether or not the target site is vacant, and least likely to move under the case (2) scenario, with by far the most number of aborted motility events possible. These intuitive predictions are confirmed by noting that $J_1 \sim -v(1-L)$, $J_2 \sim -v(1-L)^v$, and $J_3 \sim -(1-L)$ in the dense limit $L \to 1^-$.

The PDE [Eq. (33)] in the four cases Eqs. (34)–(37) has exact solutions [40], which can be written implicitly as $L = L(\xi,0)$, where $\xi = x + vt$ for case (0), $\xi = x + v(1-2L)t$ for case (1), $\xi = x + v(1-L)^{v-1}[1-(1+v)L]t$ for case (2), and $\xi = x + [(1+v)(1-L)^v - 1]\,t$ for case (3). (We have used these solutions as a check on our numerical scheme described in Sec. II B.) Written in this way, we can observe the effect each crowding case has on a given agent density profile. For example, for case (1) at a given time, each point on a profile of $L(x,t)$ moves to the left with velocity $v(1-2L)$. Thus points on the profile for which $L < 1/2$ move to the left, while points for which $1/2 < L < 1$ move to the right. This may seem counterintuitive, as all agents are left moving; thus we must be careful how to interpret the evolution of these profiles. For a Gaussian-type initial condition [Eq. (5) with $w > 1/2$] points on the right-hand tail correspond to agents in a low-density region that are moving in the $-x$ direction and so are moving into a region with a higher agent density. Thus, as time evolves, the agent density immediately to the right of x_c increases, while the agent density at x_c itself decreases. The result is that the agent density profile appears to move to the right near x_c, when in fact the agents themselves are moving to the left. Similar observations can be made for cases (2) and (3).

In the special case where $\Lambda = 0$, the nonlinearity in Eqs. (33) and (37) gradually causes an increase in the magnitude of the slope to the right of the peak, with the profiles ultimately forming a shock at some finite time [40]. For times just before the shock forms, we expect our PDE models to break down, as they are based on the assumption that $\partial L/\partial x = O(1)$. However, as we have shown in Fig. 7, we find the PDE models accurately reflect the average behavior of the simulations for small and moderate times. We also note that in the most general case with $\Lambda > 0$, such as the results shown in Fig. 8, we expect that turning events would regularize shock formation and our assumption that $\partial L/\partial x = O(1)$ is valid.

VII. DISCUSSION

In this paper we have introduced three different forms of crowding interactions into a one-dimensional velocity-jump model. The key result is that the details of the crowding interactions lead to differences in the relevant macroscopic PDE models that we have derived and validated here. This means that, unlike position-jump models, the macroscopic PDEs for a traditional noninteracting velocity-jump model are very different from the macroscopic PDE models for a velocity-jump process that includes crowding effects.

In Figs. 7(g) and 7(h) we compare the solution of the PDE governing a traditional noninteracting velocity-jump process and the solutions for the three interacting velocity-jump processes for a particular problem with $\lambda = 0$. We see that the noninteracting profile has moved farther in the $-x$ direction than any of the interacting profiles, meaning that the crowding effects introduced in the interacting models act to decrease the net motility of agents in the system.

The differences between the interacting and noninteracting models have some obvious and important consequences. For example, if we were to apply a traditional noninteracting velocity-jump model to interpret a cell migration assay where crowding effects are present, then we would expect that any calibration process used to match the experimental results to the solution of the noninteracting model would lead to an incorrect estimation of the parameters in the problem. By comparing the discrepancy between the interacting and noninteracting profiles in Figs. 7(g) and 7(h), we see that this discrepancy increases as t increases with a very large

discrepancy after 100 time steps. The interacting and noninteracting profiles in Figs. 8(g) and 8(h) for $\lambda > 0$ show the exact same trends. Note that in Figs. 8(g) and 8(h) we only present results for the left-moving subpopulation and that the continuum profiles $L(x,t)$ for interacting cases (1)–(3) are almost indistinguishable from each other, whereas the continuum profile for the noninteracting model, case (0), is very different.

Although we observe a very large discrepancy between the solutions of the interacting and noninteracting models in Figs. 7 and 8, we note that the differences between the profiles among the three interacting models is relatively small. This can be explained by considering the relationship between the three interacting cases. For example, setting $v = 1$ in cases (2) and (3) means that the governing PDEs simplify to give the same PDEs that we have for interacting case (1). Furthermore, we note that the differences between the PDEs for cases (1) and (2) will increase as v increases. For case (3) we have a more complicated crowding factors in the PDEs [Eqs. (31) and (30)] and it is more difficult to see a relationship between case (3) and the other cases.

The accuracy of all PDE models derived in this paper depends on the accuracy of the truncated Taylor series used to relate the average occupancy of lattice sites Eqs. (10) and (11). The error term in the truncated Taylor series is proportional to $O(v\tau)$, which means that we expect the quality of the continuum-discrete match to degrade as v increases. We chose to present all simulation data and continuum-discrete comparisons in this work for $v = 2$ in order to balance two competing effects. First, this was the smallest value of v for which the PDE descriptions of the three interacting velocity-jump models are different [had we chosen $v = 1$, then the PDE descriptions of cases (1)–(3) would have been identical]. Second, we chose to set $v = 2$ instead of a much larger value of v since we know that the truncated Taylor series are more accurate when v is small. For completeness, we also generated simulation data, density profiles, and made continuum-discrete comparisons for larger values of v (e.g., $v = 3,5$) and observed a reasonably good match between the continuum and discrete profiles for these additional larger values of v; however, these additional results are not reported here.

VIII. CONCLUSION

In summary, the key focus of our work has been to introduce and analyze three different forms of crowding effects in a velocity-jump process to show that the relevant governing macroscopic PDE description of the system depends on the form of crowding interactions introduced into the discrete model. Although our main aim has been to extend the traditional noninteracting velocity-jump process to incorporate crowding effects, it should also be possible to introduce many other biologically motivated mechanisms into the discrete model, including agent proliferation [17], agent death [20], agent-to-agent adhesion [15,41,42], and agents of different shapes and sizes [43]. A similar procedure could be implemented for any of these additional mechanisms to arrive at the governing PDE model for these more complex discrete mechanisms. Other extensions could include considering two- and three-dimensional transport processes or more general turning kernels [21] and a distribution of possible velocities instead of motion at a constant speed.

ACKNOWLEDGMENT

S.W.M acknowledges support from the Australian Research Council through the Discovery Project No. DP0878011.

[1] H. C. Berg, *Random Walks in Biology* (Princeton University Press, Princeton, 1983).
[2] E. A. Codling, M. J. Plank, and S. Benhamou, J. R. Soc. Interface **5**, 813 (2008).
[3] J. D. Murray, *Mathematical Biology I: An Introduction*, 3rd ed. (Springer-Verlag, Heidelberg, 2002).
[4] M. J. Simpson, A. Merrifield, K. A. Landman, and B. D. Hughes, Phys. Rev. E **76**, 021918 (2007).
[5] R. E. Baker, C. A. Yates, and R. Erban, Bull. Math. Biol. **72**, 719 (2009).
[6] B. H. Berg and D. A. Brown, Nature (London) **239**, 500 (1972).
[7] P. K. Maini, D. L. S. McElwain, and D. I. Leavesley, Tissue Eng. **10**, 475 (2004).
[8] M. Ward, C. McCann, M. DeWulf, J. Y. Wu, and Y. Rao, J. Neurosci. **23**, 5170 (2003).
[9] A. Q. Cai, K. A. Landman, and B. D. Hughes, J. Theor Biol. **245**, 576 (2007).
[10] N. R. Druckenbrod and M. L. Epstein, Dev. Dyn. **236**, 84 (2007).
[11] M. J. Simpson, K. A. Landman, and B. D. Hughes, Physica A **388**, 399 (2009).
[12] T. M. Liggett, *Stochastic Interacting Systems: Contact, Voter and Exclusion Processes* (Springer-Verlag, Berlin, 1999).
[13] L. M. Sander and T. S. Deisboeck, Phys. Rev. E **66**, 051901 (2002).
[14] K. J. Painter and T. Hillen, Can. Appl. Math. Q. **10**, 501 (2002).
[15] C. Deroulers, M. Aubert, M. Badoual, and B. Grammaticos, Phys. Rev. E **79**, 031917 (2009).
[16] E. Khain, M. Katakowski, S. Hopkins, A. Szalad, X. Zheng, F. Jiang, and M. Chopp, Phys. Rev. E **83**, 031920 (2011).
[17] T. Callaghan *et al.*, J. Stat. Phys. **122**, 909 (2006).
[18] E. Khain, L. M. Sander, and C. M. Schneider-Mizell, J. Stat. Phys. **128**, 209 (2007).
[19] J. M. Bloomfield *et al.*, J. R. Soc. Interface **7**, 1525 (2010).
[20] M. J. Simpson and R. E. Baker, Phys. Rev. E **83**, 051922 (2011).
[21] R. Erban and H. Othmer, SIAM J. Appl. Math. **65**, 361 (2004).
[22] S. Goldstein, Q. J. Mech. Appl. Math. **4**, 129 (1951).
[23] M. Kac, Rocky Mount. J. Math. **4**, 497 (1974).
[24] C. Patlak, Bull. Math. Biophys. **15**, 311 (1953).
[25] A. Okubo and S. A. Levin, *Diffusion and Ecological Problems: Modern Perspectives* (Springer, Berlin, 2001).

[26] V. V. Tetz, O. V. Rybalchenko, and G. A. Savkova, FEMS Microbiol. Lett. **107**, 231 (1993).
[27] T. Surrey, F. Nedelec, S. Leibler, and E. Karsenti, Science **292**, 1167 (2001).
[28] A. Snezhko, K. Barlan, I. S. Aranson, and V. I. Gelfand, Biophys. J. **99**, 3216 (2010).
[29] T. Vicsek, A. Czirok, E. Ben-Jacob, I. Cohen, and O. Shochet, Phys. Rev. Lett. **75**, 1226 (1995).
[30] I. D. Couzin, J. Krause, N. R. Franks, and S. A. Levin, Nature (London) **433**, 513 (2005).
[31] B. D. Hughes, *Random Walks and Random Environments*, Vol. 1 (Oxford University Press, New York, 1995).
[32] M. J. Simpson and K. A. Landman, Adv. Water Resour. **30**, 2026 (2007).
[33] M. J. Simpson, K. A. Landman, and T. P. Clement, Math. Comput. Simulat. **70**, 44 (2005).
[34] A. Schadschneider, Physica A **313**, 153 (2002).
[35] D. Chowdhury, A. Schadschneider, and K. Nishinari, Phys. Life Rev. **2**, 318 (2005).
[36] M. J. Simpson, K. A. Landman, and B. D. Hughes, Physica A **389**, 3779 (2010).
[37] S. C. Chapra and R. P. Canale, *Numerical Methods for Engineers* (McGraw-Hill, New York, 1998).
[38] C. Zheng and G. D. Bennett, *Applied Contaminant Transport Modeling*, 2nd ed. (Wiley, New York, 2002).
[39] T. Hillen and H. Othmer, SIAM J. Appl. Math. **61**, 751 (2000).
[40] G. B. Whitham, *Linear and Nonlinear Waves* (Wiley, New York, 1974).
[41] M. J. Simpson, K. A. Landman, B. D. Hughes, and A. E. Fernando, Physica A **389**, 1412 (2010).
[42] M. J. Simpson, C. Towne, D. L. S. McElwain, and Z. Upton, Phys. Rev. E **82**, 041901 (2010).
[43] M. J. Simpson, R. E. Baker, and S. W. McCue, Phys. Rev. E **83**, 021901 (2011).